Optical imaging and pH-awakening therapy of deep tissue cancer based on specific upconversion nanophotosensitizers

Yansong Feng[a], Haoran Chen[b], Yanni Wu[a], Ivo Que[c], Filippo Tamburini[c], Fabio Baldazzi[c], Yulei Chang[b,**], Hong Zhang[a,*]

[a] Van 't Hoff Institute for Molecular Sciences, University of Amsterdam, Science Park 904, 1098XH, Amsterdam, the Netherlands
[b] State Key Laboratory of Luminescence and Applications, Changchun Institute of Optics, Fine Mechanics and Physics, Chinese Academy of Sciences, Changchun, 130033, Jilin, China
[c] Translational Nanobiomaterials and Imaging, Department of Radiology, Leiden University Medical Center, 2333, ZA, Leiden, Netherlands

ABSTRACT

Side effect is one of the main factors affecting the success of cancer therapies in clinic. Patients treated with photodynamic therapy (PDT) suffer mainly from the phototoxicity due to the relatively long time blood circulation of the tumor enrichment and they have also to be protected from background light for days after the treatment. Here we introduce a new design of nanophotosensitizers in which the luminescence upconversion nanoparticles loaded with photosensitizers are self-assembled into a nanoball with the aid of a specific pH-sensitive polymer layer containing overloaded photosensitizers and quenching molecules. This design makes the therapy function "off/on" possible, i.e. only imaging during the circulation of the nanoballs ascribing to the near-infrared (NIR) photon upconversion of the nanoballs and the pH-sensitive shell. Activation of PDT solely occurs once the nanoballs are taken up by the cancer cells due to the acidic microenvironment. This design prevents effectively the photodamage of the photosensitizers during enrichment and targeting process of tumor, as validated *in vitro* and *in vivo*, which enables imaging-guided PDT treatment of deep-seated tumor in a much more relax and comfortable way for patients. This patient-friendly nanomaterial construction strategy can also be extended to other therapies.

1. Introduction

Current cancer therapies are confronted with various challenges despite the great progress in targeting efficiency of past decade [1–4]. Photodynamic therapy (PDT), for example, as a non-invasive methodology in clinic [5–7] is concerned with the phototoxicity of normal tissue during the course triggered by surrounding light, *i.e.* PDT is in "always-on" mode [8–11], (2) limited tissue penetration depth due to the excitation requirement of the UV/Visible light [12,13], and (3) poor tumor accumulation [14,15]. With the advance of nanotechnology, theranostic nanoplatforms wherein imaging and PDT are integrated into a smart "all-in-one" platform have become possible which improves the efficacy of this methodology [16–19]. The power of these new theranostic nanoplatforms is, however, often reduced by the deleterious photoactivation during their blood circulation. In order to minimize the phototoxicity in non-therapeutic process, controlled activation of therapy, *i.e.* "off-on" strategy, with therapy subject to tumor

and/or intracellular microenvironments, such as pH, glutathione, or enzymes, has been introduced [20–22]. Majority of the nanoplatforms are based on organic fluorescent molecules or polymer photosensitizers (PSs) in which the excitation of visible light limits the penetration depth. More critically, the fluorescence used for imaging/diagnosis has to be abandoned in order to avoid PDT effect before enrichment in the lesion area. On the contrary, near-infrared (NIR) light responsive inorganic upconversion nanoparticles (UCNPs) capable of converting the NIR photons to UV and/or visible photons are regarded as a very promising candidate of theranostic nanoplatforms to improve the cancer imaging and curative effect of the PDT at deep tissues [17,23,24]. Upconversion nanoplatform owns the merit of stable emission of high specificity and narrow bands, deep tissue penetration since the NIR excitation falls in the optical biological window [25–27], minimal autofluorescence background, much less light scattering compared to UV/visible light and low photodamage of tissue. Nowadays, study of PDT oriented UCNPs focuses on two aspects. One is to improve the

therapeutic efficacy, *e.g.* via enhancing the energy transfer efficiency between UCNPs and PSs and/or joint effect of PDT with other therapies and/or manipulating the tumor microenvironment [28–30]. The other is to improve the biosafety of PDT, *e.g.* thermal effect control *via* excitation wavelength adjusting from 980 nm to 800 nm, engineering UCNPs as drug carriers to improve the drug delivery efficiency [31–34]. However, important deleterious phototoxicity of UC photosensitizers arising from their unavoidable nonspecific targeting and the photoactivities of PSs induced by background light or self-catalyzed reactions has not yet been well documented and circumvented [35,36]. One solution is to follow so-called "off-on" strategy, which means that the therapy function is off in non-theraprutic process and is triggered on when necessary via external stimuli. For cancer therapy pH-sensitive "off-on" is especially interesting due to the acidic internal environment of cancer cells. Recent report of pH-responsive PDT based on UCNPs relies on self-assembly of a large amount of the nanoparticles and PSs shelled by a pH-sensitive polymer layer forming a ball [37]. Photoactivity is thus quenched due to the high concentration of PS within the shell, which can be activated once the ball is inside the intracellular tumor endo/lysosome where the acidity environment disassembles the polymer shell releasing the individual UCNP and free PSs. Such an interesting approach, however, remains some key drawbacks, *e.g.* large ball size would lead to rapid uptake by mononuclear phagocytic system and the circulation time is thus greatly curtailed. Besides, the released UCNP and free PSs have uncontrolled distance in between which is deleterious for an effective energy transfer between the UCNP and PSs. In our previous report, a photoswitching approach based on the excitation wavelength dependence of PDT was proposed and validated to be effective in minimizing the negative phototoxicity of upconversion nanophotosensitizers [38]. Herein, based also on the pH sensitivity of cancer cells, we explore further the possibility that the therapeutic effect is diminished greatly in blood circulation for diagnosis/imaging and is efficiently activated once in the intracellular microenvironment, which shall facilitate greatly the potential clinic application of the relevant materials in cancer treatment.

The nanostructure, named as tumor-intracellular sensitive photodynamic nanoplatforms (TISPNs) in this paper, is based on the high pH-sensitivity of a precisely self-assembled PEGylation quenching polymer shell. Being more specific, the TISPNs keeps photoactivity silent for the diagnosis/imaging at pH 7.4 in blood circulation, once TISPNs are uptaken by cancer cells, photoactivity will be awakened due to the acidity of the intracellular endocytic vesicles which dissociates the protective polymer shell and assists the endo/lysosome escape of recovered UCNP-based nanophotosensitizer to different organelles for efficient PDT. In order to avert effectively the generation of singlet oxygen and other reactive oxygen species (ROS) in blood circulation a joint effect of concentration quenching of the photosensitizers and robust upconversion luminescence (UCL) quenching of the polymers is specifically designed for the polymer shell (*cf* Fig. 1a). This design guarantees a highly efficient energy transfer from upconversion nanoparticles to photosensitizers via nonradiative resonant energy transfer once uptaken by the cancer cells, far superior to the previously reported simple mixture of the nanoparticle and photosensitizers [37]. The power of this approach is validated *in vitro* and *in vivo* as proof of principle.

2. Experimental section

2.1. Reagents

$RECl_3 \cdot 6H_2O$ (Re: Y, Yb, Er $>$ 99%), oleic acid (90%), 1-octadecene (ODE, 90%), oleylamine (70%), CF_3COONa, $(CF_3COO)_3Y$, rose bengal, NaOH, NH_4F, CH_3O-PEG-OH, TEA, α-bromoisobutyryl bromide, Na_2SO_4, DPA-MA, PMDETA, CuBr, DMF, dimethyl sulphoxide (DMSO), THF, 2-propanol, dichloromethane, methanol, ethanol, acetone and cyclohexane were purchased from Sigma-Aldrich. Black hole quencher

(BHQ) was purchased from Biosearch Technologies. All the chemicals were of analytical grade and were used without further purification. The cell lines used in this study were obtained from Leiden University Medical Center.

2.2. Synthesis of Me-PEG-Br

CH_3O-PEG-OH (10 g, 2 mmol) and TEA (0.7 mL, 5 mmol) were dissolved in 100 mL dichloromethane and settled in an ice bath. α-bromoisobutyryl bromide (0.63 mL, 5 mmol) dissolved in 5 mL dichloromethane was added dropwise under argon. After stirring for 24 h at room temperature, the solution was washed with 1 M NaOH (3 × 20 mL) and 1 M HCl (3 × 20 mL) and water (3 × 20 mL). After drying with anhydrous Na_2SO_4, the solution was concentrated to about half of its original volume through evaporation, and ether was added to precipitate the product. After recrystallization thrice and drying under vacuum, the product was collected as white powder.

2.3. Synthesis of PEG-b-(PR-r-RB) and PEG-b-(PR-r-BHQ)

PEG-b-(PR-r-AMA) was synthesized by atom transfer radical polymerization (ATRP) method. DPA-MA (1.06 g, 5 mmol), PMDETA (21 μL, 0.1 mmol), and Me-PEG-Br (0.5 g, 0.1 mmol) were charged into a polymerization tube, followed by adding a mixture of 2-propanol (2 mL) and DMF (2 mL) to dissolve the monomer and initiator. After degassing to remove oxygen, CuBr (14 mg, 0.1 mmol) was added into the reaction tube under argon atmosphere, and the tube was then sealed in vacuum. The reaction was stirred at 40 °C overnight. The reaction mixture was diluted with 10 mL THF and passed through an Al_2O_3 column to remove the catalyst. The THF solvent was removed by rotovap. The residue was dialyzed in distilled water and lyophilized to obtain white powder.

For RB or BHQ conjugation, 50 mg of PEO-b-(PR-r-AMA) was mixed with RB hexanoic acid (RB-HA) or BHQ-COOH (1.5 equivalents to the molar amount of the primary amino group), NHS and EDC-HCl in 2 mL of anhydrous DMF. The reaction mixture was stirred at room temperature for two days. The polymer conjugates were purified by preparative gel permeation chromatography to remove the free dye molecules. The resulting polymer conjugates were lyophilized and stored at −20 °C.

2.4. Preparation of NaYF₄ precursor

Typically, 2 mmol CF_3COONa and 2 mmol $(CF_3COO)_3Y$ were added into a 100 mL flask with 6 mL oleic acid, 6 mL oleylamine and 10 mL 1-octadecene. Under nitrogen the mixture was heated to 65 °C with stirring for 30 min to dissolve the reagents. The solution was then heated to 290 °C and reacted for 1 h. After the reaction it was cooled down to room temperature. The obtained precursor was centrifuged for 5 min with 6000 rpm and washed with ethanol and finally dispersed in 16 mL 1-octadecene.

2.5. Synthesis of NaYF₄: 2% Er, 20% Yb @ NaYF₄ nanoparticles

In a typical experiment, 0.78 mmol $YCl_3 \cdot 6H_2O$, 0.20 mmol $YbCl_3 \cdot 6H_2O$ and 0.02 mmol $ErCl_3 \cdot 6H_2O$ were added in a 100 mL three-neck flask with 6 mL oleic acid and 15 mL 1-octadecene. The solution was stirred for 60 min under argon atmosphere and then heated to 160 °C until the $ReCl_3$ were dissolved. It was then cooled down to room temperature, and after the addition of 5 mL methanol solution containing 2.5 mmol NaOH and 4 mmol NH_4F the clear solution turned into opacity and was heated to 70 °C for 30 min to remove the methanol. Afterwards the solution was rapidly heated to 300 °C reacted 60 min with stirring under an argon atmosphere, then injected 4 mL $NaYF_4$ solution prepared before and reacted for another 30 min. The resulting nanoparticles were washed with acetone and then washed
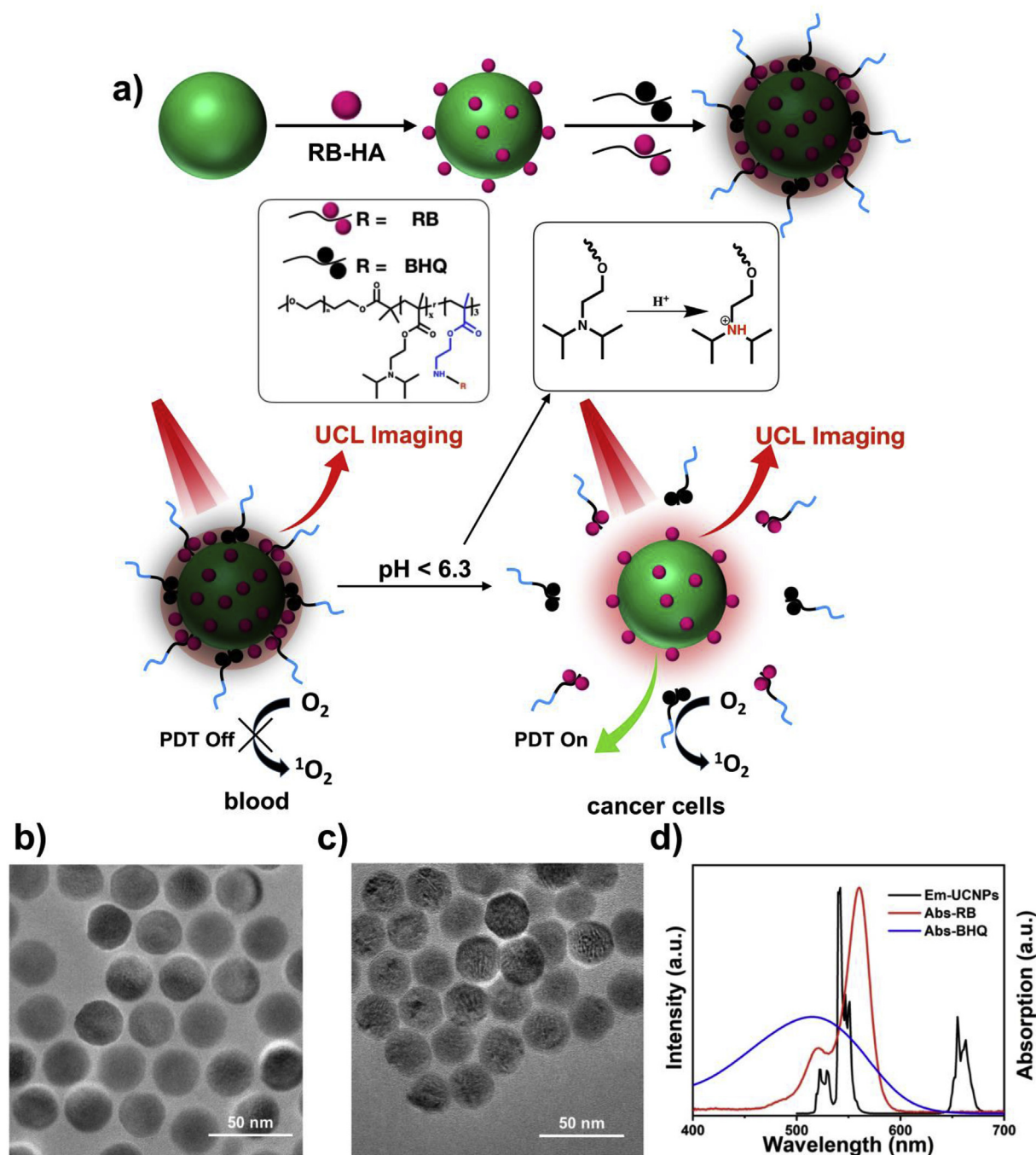
Fig. 1. a) Schematic illustration of pH-sensitive PDT of TISPNs and relevant preparation procedure. The TEM images of b) UCNPs-OA, and c) TISPNs. d) UCL spectrum of UCNPs under 980 nm light excitation (in black); absorption spectra of photosensitizer RB (in red) and black hole quencher (BHQ, in blue). (For interpretation of the references to colour in this figure legend, the reader is referred to the Web version of this article.)

with ethanol twice, and finally dispersed in 4 mL cyclohexane.

2.6. Preparation of UCNPs-RB

The hydrophobic UCNPs solution (~10 mg in 2 mL of cyclohexane) was mixed with different amounts of RB-HA, and adding 2 mL THF, the solution was stirred vigorously over 24 h at room temperature. UCNPs-RB nanoplatforms was then centrifuged and washed with acetone and DMSO to remove any unreacted RB-HA. The obtained UCNPs-RB were redispersed in DMSO for further use.

2.7. Preparation of "Always On", "Always Off" and TISPNs

3 mg PEG-b-(PR-r-RB), 3 mg PEG-b-(PR-r-BHQ) and 0.3 mg UCNPs-RB (with the optimal loading capacity 2%) were mixed with 2 mL of DMF, followed by the addition of 2 mL pH = 9.2 phosphates buffered saline. The solution was then transferred to a dialysis bag (cut-off 3500 MW) for dialysis against pH = 9.2 buffer for 2 days. Subsequently, the as-prepared micelles were purified through centrifugation to remove the excess free polymer, then filtered with a 0.22 mm filter. Due to hydrophobic-hydrophobic interactions, this strategy is capable of producing a stable polymer shell on UCNPs-RB to form the TISPNs. For the "Always Off" nanoparticles, the preparation

route was similar to the preparation of TISPNs where the difference was that polymers used here are PEG-RB and PEG-BHQ. For the "Always On" nanoparticles, the polymer was PEG without any modification.

2.8. Singlet oxygen detection ($^1O_2$)

The amount of $^1O_2$ was determined with DPBF from the absorption at 410 nm. 2 mL of as-obtained UCNPs-RB (different amount) dispersed in water and 10 μL of DPBF-ethanol solution was added which was kept in dark overnight. The absorbance of DPBF at 410 nm was recorded every 3 min after irradiation of 980 nm laser (3, 6, 9, 12, 15 and 18 min) at the power density of 0.7 W/cm^2. For TISPNs in different pH values, TISPNs were dispersed in different pH PBS (7.4, 6.5, 6.0 or 5.5) and then added in 10 μL DPBF-ethanol solution and kept in dark overnight. The absorbance of DPBF at 410 nm was recorded every 3 min after irradiation of 980 nm laser (3, 6, 9, 12, 15 and 18 min) at power density of 0.7 W/cm^2.

2.9. PDT in vitro

Breast carcinoma MCF-7 cells were maintained in the DMEM under 5% CO$_2$ atmosphere at 37 °C. The cells were incubated in the 96-well plate (1 × 10^4 per well) for 24 h. Afterwards, TISPNs, "Always Off" or "Always On" nanoparticles were added in the cells with different concentrations (0, 50, 100, 200, 400 μg/mL), each with five parallel. The cell viability was investigated using a standard MTS assay.

Regarding the PDT effect of the TISPNs, the cells were incubated in the 96-well plates with TISPNs, "Always Off" or "Always On" nanoparticles (50, 100, 150 or 200 μg/mL) for 8 h and followed by PBS washing. The cells incubated with PBS as the control experiments, the cells only with 980 nm irradiation was for the toxicity of the laser and incubated with TISPNs but without 980 nm irradiation was for the comparison. A CW 980 nm laser was used to irradiate the cells (group "980 nm", "Always Off + 980 nm", "Always On" + 980 nm and "TISPNs + 980 nm") for 15 min at a density of 0.7 W/cm^2. After that the cells were cultured for another 48 h. The 980 nm mediated PDT efficacy was evaluated by MTS assay.

2.10. Flow cytometry

For the flow cytometry analysis, the cells were trypsinized and stained by Annexin V-FITC and propidium iodide (Annexin V-FITC Apoptosis Staining/Detection Kit) to measure the cells experiencing apoptosis. The process was executed using flow cytometry.

Annexin-V-fluorescein isothiocyanate (FITC) and propidium iodide (PI) staining were performed using an Annexin-V-FITC/PI kit (BD) according to the manufacturer's instructions. Briefly, MCF-7 cells were cultured in 6-well plates and then treated with different reagents (PBS, TISPNs, "Always Off" or "Always On" nanoparticles) for 4 h, each with 3 parallel. The cells treated with PBS were for the control. For the other three groups, each parallel was then exposed to the laser irradiation for 15 min at a density of 0.7 W/cm^2. Cells were harvested using 0.05% trypsin after 24 h incubation and washed twice with cold PBS, and suspended in binding buffer. 1 × 10^5 cells in 100 μL binding buffer were added to a tube and incubated with 5 μL of Annexin-V-FITC and 5 μL of PI. Cells were gently mixed and incubated for 15 min at room temperature. 400 μL binding buffer was then added to each tube. The samples were analyzed by flow cytometry (BD Biosciences). Experiments were repeated three times.

2.11. In vivo imaging and PDT

The mice experiments were performed in accordance with animal regulations and management protocols. The tumors were developed by the subcutaneous injection of MCF-7 cells into nude mice. When the tumor volume grew to about 50 mm^3 the mice were randomly

separated into different groups. After the post-injection of nanoplatforms, the mice were imaged with a modified IVIS system, which was equipped with a 980 nm light source. For PDT treatment, the mice were randomly divided into six groups (n = 5) (i) Saline, (ii) 980 nm light, (iii) TISPNs alone (iv) "Always Off" nanoparticles with 980 nm irradiation (v) "Always On" nanoparticles with 980 nm irradiation (vi) TISPNs with 980 nm irradiation. The mice were injected with the same doses of nanoparticles (0.65 mg/mouse) for relevant groups. For the irradiated groups, the mice were irradiated with 980 nm laser (0.6 W/cm^2 for 15 min, 3 min irradiation and 3 min interval), respectively. The tumor sizes and body weights of the mice were monitored during the 14 days of treatment. The volume of tumor was measured as Volume = (L × W [2]/2), where L (length) and W (width) are two tumor dimensions, respectively. After the various treatment, the main organs and tumor tissues of the mice were collected on the 14th day for further study after H&E staining.

2.12. Statistical analysis

Statistical data were analyzed applying one-way ANOVA test.

3. Results and discussion

3.1. Synthesis and structure characterization of TISPNs

The pH-sensitive TISPNs were constructed starting with the synthesis of core-shell structured UCNPs followed by the shielding polymer coating (Fig. 1a). Transmission electron microscopy (TEM) images shown in Fig. 1b and c and Fig. S1 confirm the average size of the oleic acid-capped monodispersive UCNPs to be ~26 nm. No obvious aggregation was observed after surface functionalization. The green UCL of UCNPs overlaps well in spectrum with the absorption of the photosensitizer rose bengal (RB) (Fig. 1d), indicating that UCNPs can be used as an energy transducer for RB photosensitization. Singlet oxygen ($^1O_2$) production of the UCNP-based nanophotosensitizer is thus dependent on nonradiative resonant energy transfer between the UCNP and RB which relies on not only the spectral overlap between the emission of UCNPs and the absorption of PSs but also the energy transfer distance and the amount of PS molecules loaded on each UCNP [39,40]. The optimal amount of PSs anchored on the surface of UCNPs corresponding to the best PDT efficacy was determined from the influence of RB loading capacity on the $^1O_2$ production. It was found that with the increase of RB the green UCL (~520–540 nm) decreased and the fluorescence of RB around 580 nm increased, which shifted to ~600 nm when the ratio of RB versus UCNP was over 3% (w/w) (Fig. 2a), due to the formation of dimers when there were more RB molecules attached on the UCNP. The corresponding $^1O_2$ production was measured from the absorption of the chemical probe 1, 3-diphenylisobenzofuran (DPBF) [41] (Fig. 2b and Fig. S2), where the optimal loading capacity of RB was determined to be 2% (w/w). The nanophotosensitizer constructed with optimal loading of RB was inert to the pH of the environment and named as "Always On". To make the nanophotosensitizers sensitively respond to tumor intracellular acidic environment a specific polymeric shell was coated. To this end, PSs quenchers (PSQ), PEG-b-(PR-r-RB) and PEG-b-(PR-r-BHQ) (Fig. 1a), were prepared by conjugating PEG-b-(PR-r-AMA) with RB and black hole quencher (BHQ), respectively. TISPNs were constructed via a self-assembly approach with details provided in Supporting Information. Free amphiphilic polymers were removed by centrifugation. Compared with the freeloading approach, the conjugation of RB and BHQ with PEG-b-(PR-r-AMA) theoretically avoids the payloads leaking from the hydrophobic layer before taken up by the tumor cells since they experience neutral environment in which the polymer shell is stable. Cellular uptake of TISPNs changes their surroundings from neutral (pH~7.4) to acidic (pH < 6.3) resulting in the dissociation of the shielding polymer shell. This picture was supported by the results of DLS and emission spectra of
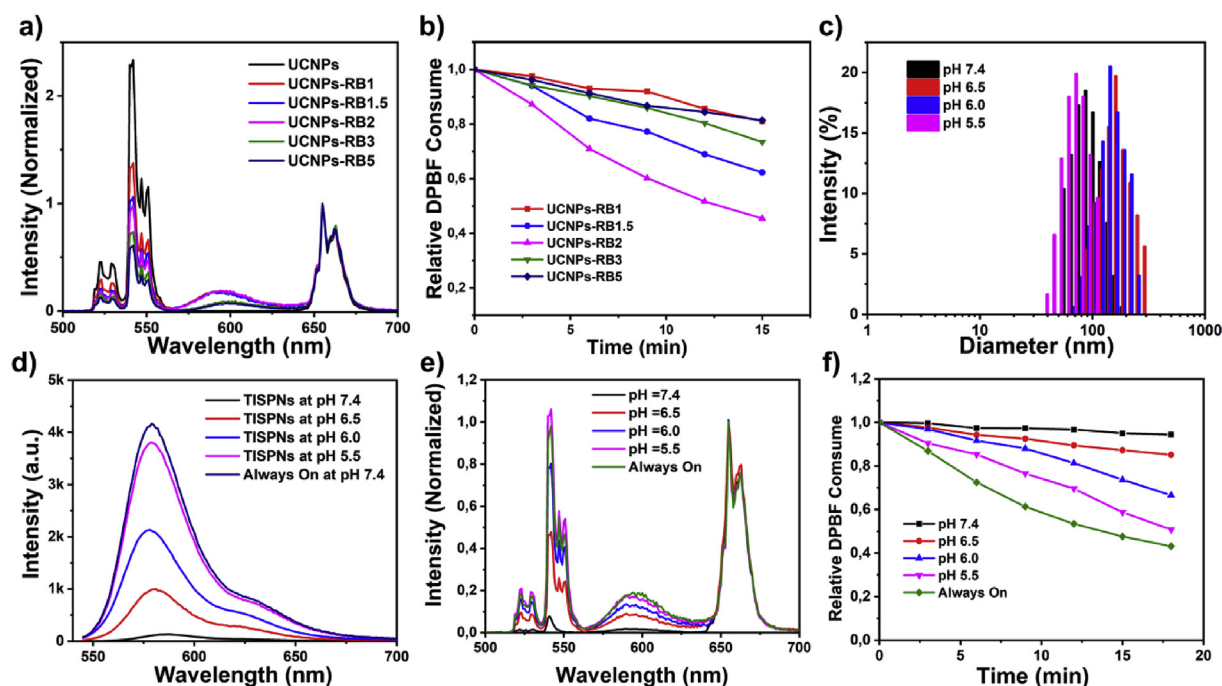
Fig. 2. a) UCL spectra of UCNPs loading with different amounts of RB. b) The DPBF consumption with time treated with UCNPs loading with different amounts of RB under 980 nm light irradiation. c) The hydrodynamic size of TISPNs at different pH value. d) Fluorescence intensity of RB from TISPNs at different pH value or from "Always On" at pH 7.4. Excitation was at 540 nm. e) UCL spectra of TISPNs at selected pH values and UCL spectram of the "Always On", excitation was at 980 nm. f) Relative DPBF consumption incubated with TISPNs at selected pH values and "Always On" upon 980 nm light irradiation.

the nanophotosensitizer. Upon the modification with PSQ, the hydrodynamic diameter of TISPNs was about 102 nm (Fig. 2c) at pH 7.4, and when the pH decreased to 6.5, the PSQ swelled and the hydrodynamic diameter increased to ~172 nm. Once the pH decreased to ~6.0, the PSQ quickly reversed the charge to positive because of the ionization of the diisopropylamine groups (pKa ≈6.3), resulting in the partial dissociation of the shielding PSQ polymers. When the pH further decreased to 5.5 the hydrophobic interactions became weaker than the repulsive force between ionized unimers, complete dissociation occurred as witnessed by the smaller hydrodynamic diameter ~68 nm (UCNPs-RB). The photosafety of TISPNs was studied under the direct excitation at 540 nm as shown in Fig. 2d where the fluorescence intensity of PSs was substantially quenched (~98%) compared to the fluorescence of the conventional sample "Always On" under pH 7.4. This result reinsures the remarkable reduction of the negative phototoxicity induced by the background light, *e.g.* the sunshine, indicating the superior photosafety of TISPNs structure. While more than 90% fluorescence recovery of RB upon 540 nm light irradiation when the pH decreased to 5.5 (Fig. 2d). The disassembly process was in line with the UCL decrease around 540-520 nm and the corresponding fluorescence recovery of RB in a more acidic environment upon 980 nm irradiation (Fig. 2e).

3.2. $^1O_2$ production

In order to study the pH-mediated PDT profiles, the pH dependence of the $^1O_2$ production subject to NIR light irradiation was systematically studied. As shown in Figs. 2f and S3, the DPBF consumption declined only slightly upon NIR light irradiation of the UCNPs aqueous solution at pH 7.4. The decline was getting pronounced with the acidity of the solution and reached ~50% at pH 5.5 within 18 min. These data support the feasibility of the pH-activated PDT of the TISPNs in specific acidic intracellular cancer treatment.

3.3. 3. UCL imaging and pH-activated PDT in vitro

To verify the UCL imaging-guided intracellular pH-activated PDT of

TISPNs, we started with evaluating its dark cytotoxicity by incubating the cancer cells of MCF-7 with TISPNs. The cell viability shown in Fig. S4 is more than 85% even with a relatively high concentration of the nanoplatforms (400 μg/mL). The stability of TISPNs in the PBS buffer (pH 7.4) and cell culture medium (pH 7.4) were also investigated and the results are shown in Fig. S5, where the UCL intensity and the green to red ratio of spectra are stable in the above media, indicating silent photoactivity of TISPNs during the circulation. The UCL imaging profiles at different pH conditions were also recorded. Fig. 3 is the cell imaging profiles of MCF-7 cells in which the nuclei were stained by DAPI, and the red or green UCL images are from the TISPNs irradiated with 980 nm laser. The well overlaps of the images of the cells that incubated in 2 h and 4 h at pH 5.5 and 7.4 are a sign of effective cellular internalization of the TISPNs irrelevant of acidity of the culture medium. Interestingly, once taken up by the MCF-7 cells the quenched green UCL of the sample incubated at pH 7.4 is recovered and its intensity is comparable to that incubated at pH 5.5, in line with the breaking of the polymer shell in the acidic intracellular endocytic vesicles of cancer cells, indicating the effective dissociation and activation in the acidic environment. Moreover, the stability of UCNPs-RB is also a necessary condition for efficient PDT due to the possibility of RB dissociates from the surface of UCNPs under strongly acidic conditions. Its stability was also tested in the simulated acidic conditions of cells at pH 6.5 or 5.5 for 12 h and 24 h, as shown in Fig. S6. We can see that the UCL intensity and the green to red ratio of spectra were stable at pH 6.5 – a sign that TISPNs was stably entrapped inside the micelles without detectable RB leakage at pH values higher than 6.5. While the UCL green emission recovery, *i.e.* green to red ratio turns higher, was observed at pH 5.5, evidencing the shedding of RB from the particles at pH 5.5. Such designed TISPNs nanoplatfrom can effectively avoid the acid dissociation. The self-assembled polymer shell not only helps to quench the photoactivity of TISPNs at pH higher than 6.5 but assist also the endo/lysosome escape of UCNPs-RB, avoiding possible damage of UCNPs-RB in acidic environment. Importantly, this design ensured the optimal photoactivity of the photosensitizers.

Next, the pH-responsive PDT efficacy of MCF-7 cells *in vitro* was
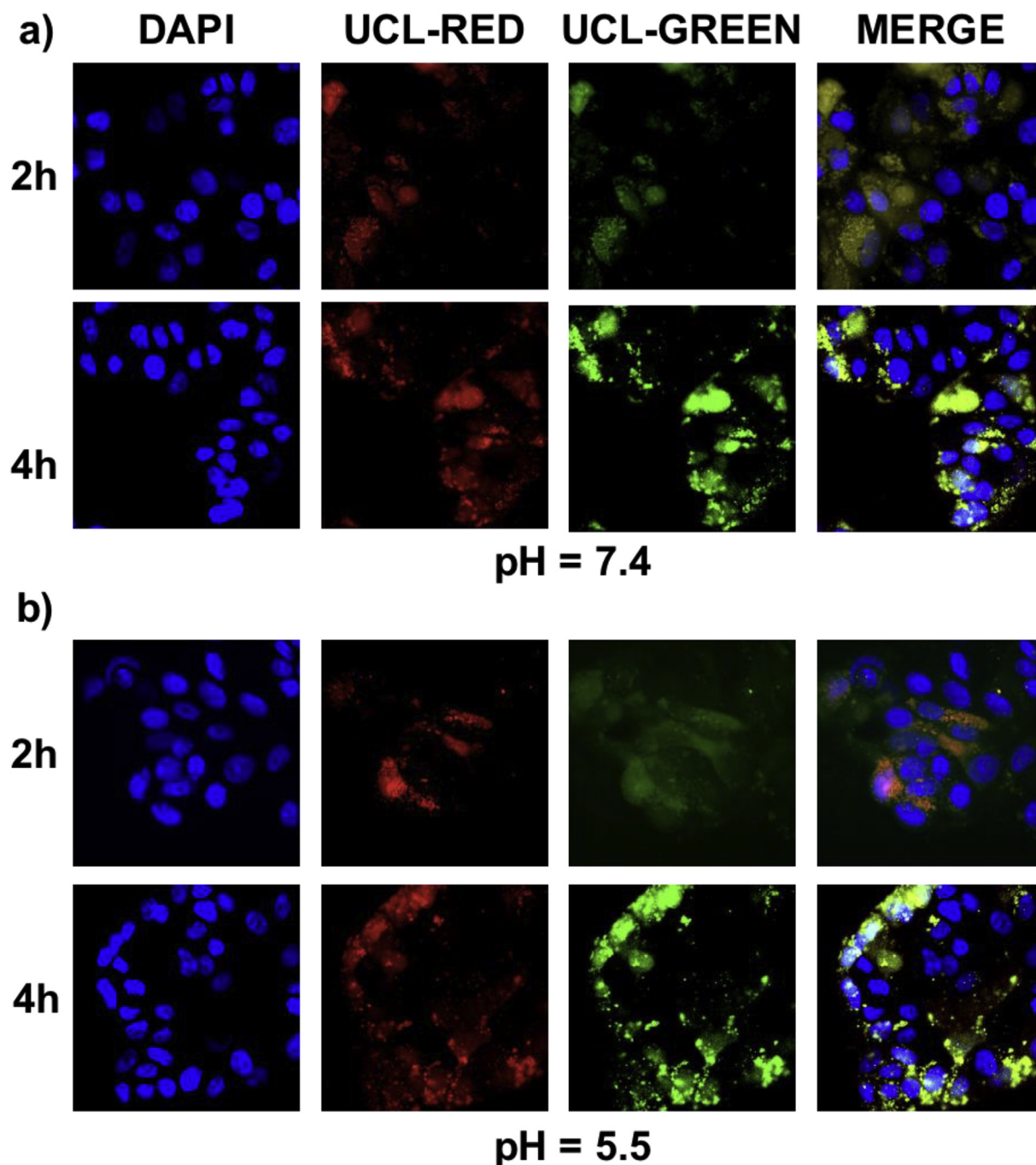
Fig. 3. MCF-7 cells were treated with TISPNs at a) pH = 7.4 or b) 5.5 for UCL imaging with 980 nm excitation, and the nuclei were stained with DAPI.

assessed by MTS assay. The UCNPs-RB/PEG (Always-on) was used as positive control and the UCNPs-RB/PEG-RB/BHQ as the negative control ("Always Off"). The cell viabilities were found to be more than 85% with groups of "saline" (treated with saline), "980 nm" (only irradiated with 980 nm light) or "TISPNs" (treated with TISPNs). Comparing the cell viabilities of groups incubated with "Always On", with "Always Off" or with TISPNs under 980 nm irradiation (Fig. 4a), it is obvious that TISPNs-incubated cells exhibited significant therapeutic effect similar to the "Always On" group (~30% viability) whereas the "Always Off" group remains ~80% viability, confirming that the phototoxicity of TISPNs was activated in the acidic intracellular endocytic vesicles of cancer cells. The cell apoptosis with the TISPNs upon NIR light irradiation was also assessed. As shown in Fig. 4b, the Annexin-V-FITC staining is for apoptotic cells and propidium iodide (PI) staining for the

necrosis cells, where there is only 54.2% viable cells and 23.9% apoptotic cells in the group treated with TISPNs, and 49.5% viable cells and 24.6% apoptotic cells in the "Always On" group. As a reference, 94.8% viable cells and only 0.37% of apoptotic cells were observed for the group "Always Off", demonstrating the negligible dark toxicity of the nanoparticles. Considering that lysosomal of normal cells is acidic which may trigger the dissociation of the polymer shell, relevant PDT effects were studied for human chondrocytes cells (C28). Results are shown in Fig. S7, it is obvious that the "off-on" strategy has improved the cell viability even for passive targeting as used in our experiments. Even through, the advantage of the "off-on" strategy is hampered to certain extent by the nonspecific uptake of normal cells. Further work is going on in our groups taking the active targeting into consideration. With the improvement of specific targeting, the photo-toxicity of "off-
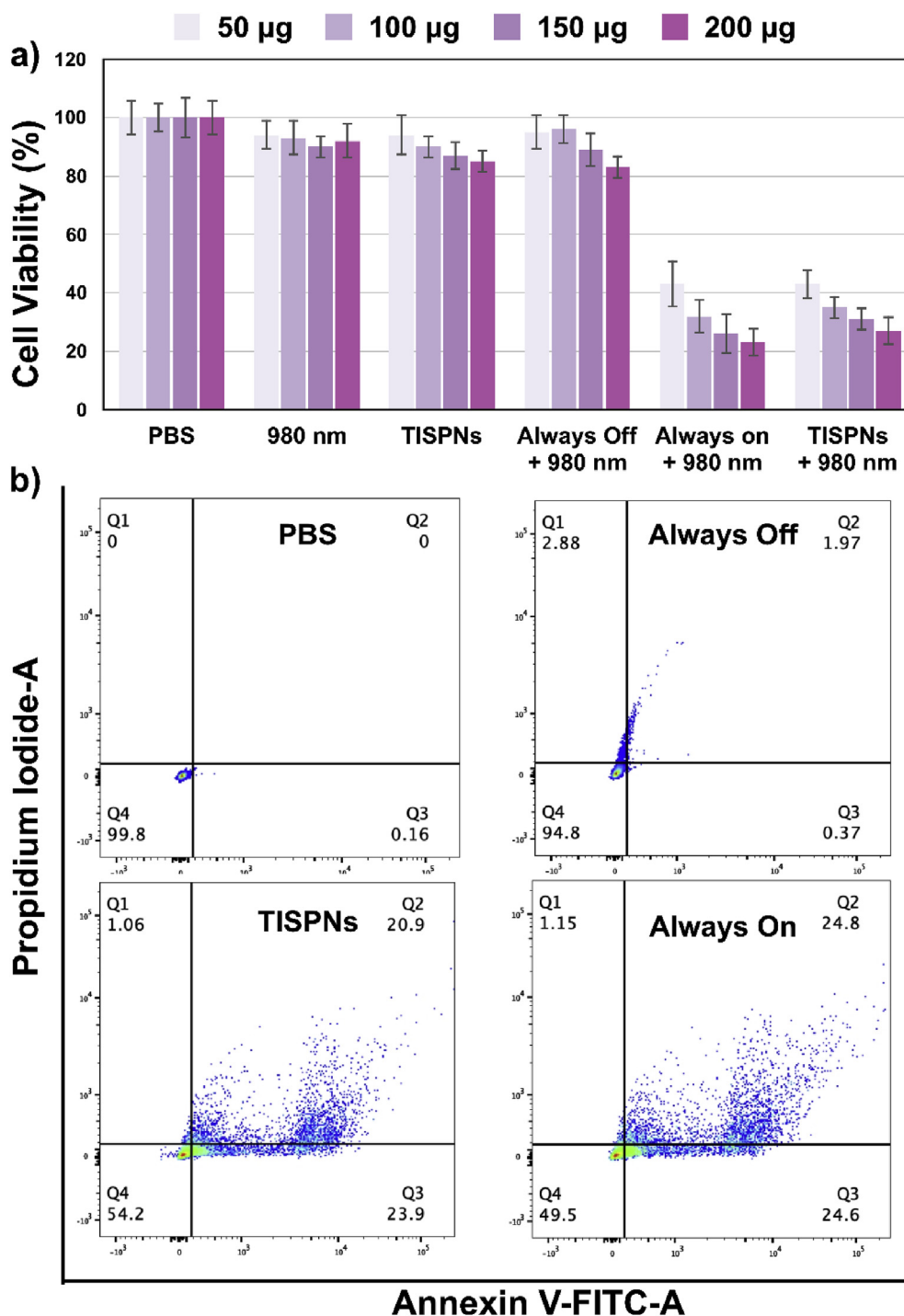
Fig. 4. a) Relative viabilities of cells for different treatment groups incubated with the PDT nanoplatforms of "Always off"; "Always on" and TISPNs at different concentrations (per mL), conducted 980 nm laser, power density = 0.7 W/cm^2 b) Apoptosis of MCF-7 cells incubated with PBS or "Always Off" or "TISPNs" or "Always On" nanoparticles, under PDT treatment. The MCF-7 cells were stained by Annexin V-FITC and analyzed by FACScan.

on" strategy is expected to be further diminished.

3.4. UCL imaging and antitumor efficacy in vivo

Reduced photoactivities during the blood circulation, tumor-specific accumulation and activation are the crucial advantages of the switchable PDT nanoplatform compared with the "Always On" nanoplatforms, which is distinctly demonstrated in UCL imaging and controlled PDT conducted on MCF-7 tumor-bearing mice. For UCL imaging, 100 μL of TISPNs (10 mg/mL) were intravenously (IV) injected into the mice and

PBS as a control. After that, the tumor-bearing mice were exposed to the 980 nm laser. The images were recorded at certain time points shown in Fig. 5a where the red UCL was detected at the tumor sites 4 h after injection which was getting stronger with time till 24 h post-injection.

The antitumor efficacy was also assessed *in vivo*. After the tumor volume grew to about 50 mm^3, the mice received various treatments, where "PBS" control group injected with PBS, "980 nm" group only with NIR laser irradiation for the light toxicity, "TISPNs" group only injected with TISPNs for the toxicity of the nanoparticles, "Always Off +980 nm" group for the PDT effect of "Always off" under 980 nm
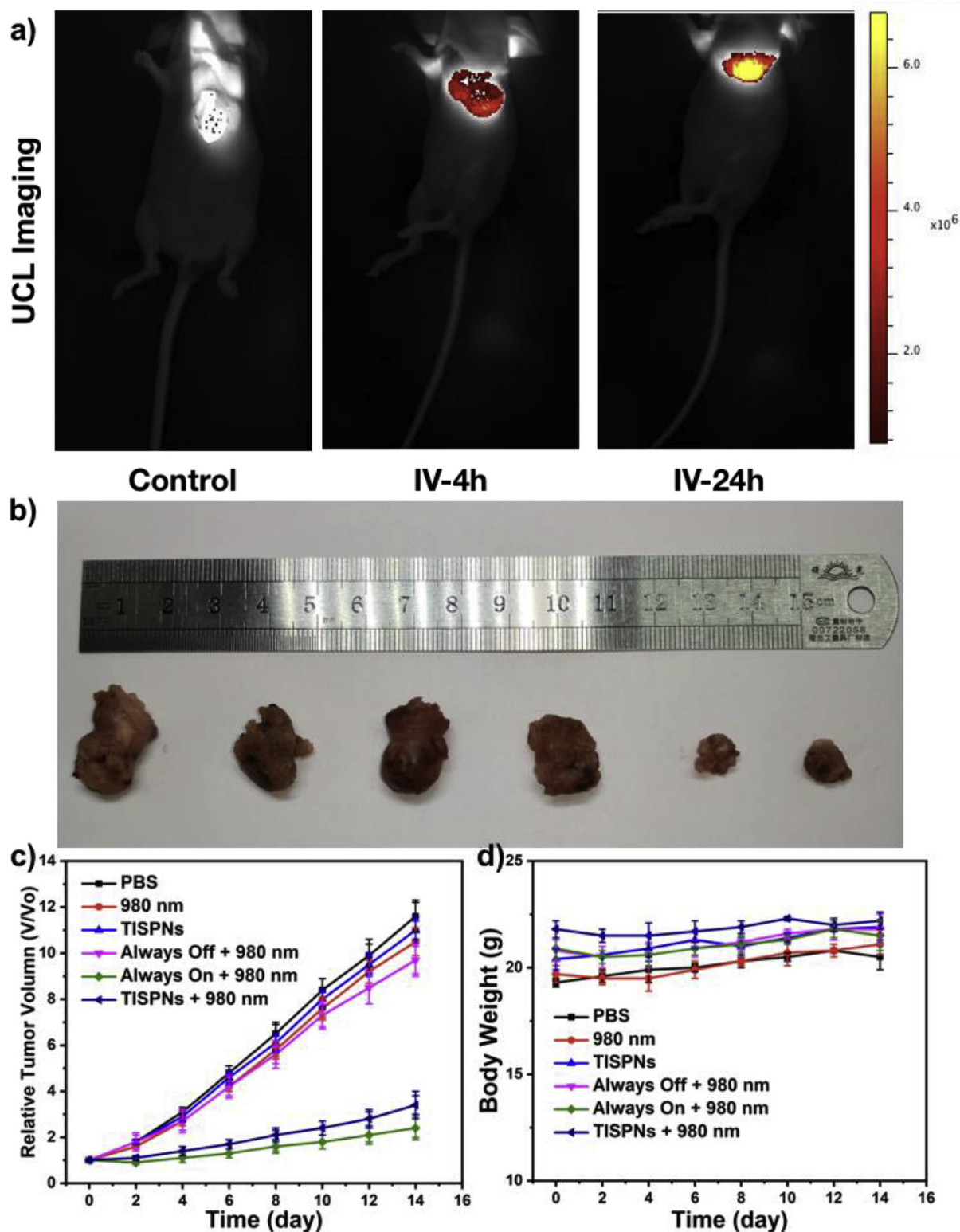
Fig. 5. a) *In vivo* UCL red imaging of tumor-bearing mouse with TISPNs under 980 nm laser after 24 h post-injection. b) Photographs to display the excised tumors after various treatment. c) Relative tumor volumes change during the treatment. d) Mice weight change during the treatment. Self-assembled pH-responsive up-conversion nanophotosensitizer make it possible for the near infrared light mediated imaging of deep tissue tumors with minimized phototoxicity of health cells. Once the nanoparticles taken up by cancer cells, photoactivity will be sw. (For interpretation of the references to colour in this figure legend, the reader is referred to the Web version of this article.)

irradiation, "Always On + 980 nm" for the PDT effect of "Always On" under 980 nm irradiation and "TISPNs +980 nm" for the PDT effect of TISPNs under 980 nm irradiation. Each mouse was injected with 65 μL (10 mg/mL) of UCNPs, and the control group for 65 μL PBS. The mice in the groups of "Always Off +980 nm", "Always On + 980 nm" and "TISPNs +980 nm" were irradiated with 980 nm laser for 15 min at 0.6 W/cm^2, respectively. The tumors were measured every two days in volume and finally excised on day 14. Results are shown in Fig. 5b and c where the TISPNs group exhibits similar high antitumor effects (71%) as the "Always On" group (79%), whereas the other treatments seem lack of sufficient inhibition effect on tumor growth as the tumors develop rapidly in these groups including the "Always Off" group. Moreover, there are no significant weight change of the mice (Fig. 5d) provides additional support of the high biosafety of this pH-switchable PDT nanoplatform. To further confirm their biocompatibility, the hematoxylin and eosin (H&E) examination were carried out (Fig. S8). Indeed, no significant damage to major organs was observed, including heart, liver, spleen, lung, and kidney in the "TISPNs" groups. On the contrary, significant damage of the tumors was observed in TISPNs group ascribed to the therapeutic effect of NIR-mediated PDT.

4. Conclusion

In summary, we have proposed and validated a novel strategy in realizing NIR upconversion imaging and cancer intracellular environment induced PDT. The *in vitro* and *in vivo* results demonstrate that this nanoplatform can achieve real-time imaging without therapeutic effect and significant tumor destructing effect is mediated by the tumor intracellular upon NIR light irradiation. This sort of materials is, therefore, a proper candidate for future precision medicine that not only surmounts the limitation of organic PSs like limited tissue penetration, autofluorescence of the physiological background and scattered light but also minimizes the side effect in normal tissues.

Declaration of competing interest

The authors declare no conflict of interest.

Acknowledgements

Appendix A. Supplementary data

Supplementary data to this article can be found online at https://doi.org/10.1016/j.biomaterials.2019.119637.

References

[1] J.M. Kane, C.U. Correll, Past and present progress in the pharmacologic treatment of schizophrenia, J. Clin. Psychiatry 71 (9) (2010) 1115–1124.

[2] H. Maeda, M. Khatami, Analyses of repeated failures in cancer therapy for solid tumors: poor tumor-selective drug delivery, low therapeutic efficacy and unsustainable costs, Clin. Exp. Med. 7 (1) (2018) 11-11.

[3] Y. Feng, Y. Wu, J. Zuo, L. Tu, I. Que, Y. Chang, L.J. Cruz, A. Chan, H. Zhang, Assembly of upconversion nanophotosensitizer in vivo to achieve scatheless real-time imaging and selective photodynamic therapy, Biomaterials 201 (2019) 33–41.

[4] W.H. De Jong, P.J.A. Borm, Drug delivery and nanoparticles:applications and hazards, Int. J. nanomedicine 3 (2) (2008) 133–149.

[5] D.E.J.G.J. Dolmans, D. Fukumura, R.K. Jain, Photodynamic therapy for cancer, Nat. Rev. Cancer 3 (2003) 380.

[6] J.P. Celli, B.Q. Spring, I. Rizvi, C.L. Evans, K.S. Samkoe, S. Verma, B.W. Pogue, T. Hasan, Imaging and photodynamic therapy: mechanisms, monitoring, and optimization, Chem. Rev. 110 (5) (2010) 2795–2838.

[7] R. Kumar, W.S. Shin, K. Sunwoo, W.Y. Kim, S. Koo, S. Bhuniya, J.S. Kim, Small conjugate-based theranostic agents: an encouraging approach for cancer therapy, Chem. Soc. Rev. 44 (19) (2015) 6670–6683.

[8] E. Reddi, Role of delivery vehicles for photosensitizers in the photodynamic therapy of tumours, J. Photochem. Photobiol., B 37 (3) (1997) 189–195.

[9] S.S. Lucky, K.C. Soo, Y. Zhang, Nanoparticles in photodynamic therapy, Chem. Rev. 115 (4) (2015) 1990–2042.

[10] J. Gao, J. Li, W.-C. Geng, F.-Y. Chen, X. Duan, Z. Zheng, D. Ding, D.-S. Guo, Biomarker displacement activation: a general host–guest strategy for targeted phototheranostics in vivo, J. Am. Chem. Soc. 140 (14) (2018) 4945–4953.

[11] X. Li, S. Kolemen, J. Yoon, E.U. Akkaya, Activatable photosensitizers: agents for selective photodynamic therapy, Adv. Funct. Mater. 27 (5) (2017) 1604053.

[12] W. Fan, P. Huang, X. Chen, Overcoming the Achilles' heel of photodynamic therapy, Chem. Soc. Rev. 45 (23) (2016) 6488–6519.

[13] A.N. Bashkatov, E.A. Genina, V.I. Kochubey, V.V. Tuchin, Optical properties of human skin, subcutaneous and mucous tissues in the wavelength range from 400 to 2000 nm, J. Phys. D Appl. Phys. 38 (15) (2005) 2543–2555.

[14] M.O. Durymanov, A.A. Rosenkranz, A.S. Sobolev, Current approaches for improving intratumoral accumulation and distribution of nanomedicines, Theranostics 5 (9) (2015) 1007–1020.

[15] V.P. Chauhan, R.K. Jain, Strategies for advancing cancer nanomedicine, Nat. Mater. 12 (2013) 958.

[16] B.Y.S. Kim, J.T. Rutka, W.C.W. Chan, Nanomedicine, N. Engl. J. Med. 363 (25) (2010) 2434–2443.

[17] N.M. Idris, M.K. Gnanasammandhan, J. Zhang, P.C. Ho, R. Mahendran, Y. Zhang, In vivo photodynamic therapy using upconversion nanoparticles as remote-controlled nanotransducers, Nat. Med. 18 (2012) 1580.

[18] E.M. Chan, E.S. Levy, B.E. Cohen, Rationally designed energy transfer in upconverting nanoparticles, Adv. Mater. 27 (38) (2015) 5753–5761.

[19] Y.I. Park, H.M. Kim, J.H. Kim, K.C. Moon, B. Yoo, K.T. Lee, N. Lee, Y. Choi, W. Park, D. Ling, K. Na, W.K. Moon, S.H. Choi, H.S. Park, S.-Y. Yoon, Y.D. Suh, S.H. Lee, T. Hyeon, Theranostic probe based on lanthanide-doped nanoparticles for simultaneous in vivo dual-modal imaging and photodynamic therapy, Adv. Mater. 24 (42) (2012) 5755–5761.

[20] D. Ling, W. Park, S.-j. Park, Y. Lu, K.S. Kim, M.J. Hackett, B.H. Kim, H. Yim, Y.S. Jeon, K. Na, T. Hyeon, Multifunctional tumor pH-sensitive self-assembled nanoparticles for bimodal imaging and treatment of resistant heterogeneous tumors, J. Am. Chem. Soc. 136 (15) (2014) 5647–5655.

[21] S. Kolemen, M. Işık, G.M. Kim, D. Kim, H. Geng, M. Buyuktemiz, T. Karatas, X.-F. Zhang, Y. Dede, J. Yoon, E.U. Akkaya, Intracellular modulation of excited-state dynamics in a chromophore dyad: differential enhancement of photocytotoxicity targeting cancer cells, Angew. Chem. Int. Ed. 54 (18) (2015) 5340–5344.

[22] J. Chen, K. Stefflova, M.J. Niedre, B.C. Wilson, J.D. Glickson, G. Zheng, Protease-triggered photosensitizing beacon based on singlet oxygen quenching and activation, J. Am. Chem. Soc. 126 (37) (2004) 11450–11451.

[23] N.M. Idris, M.K.G. Jayakumar, A. Bansal, Y. Zhang, Upconversion nanoparticles as versatile light nanotransducers for photoactivation applications, Chem. Soc. Rev. 44 (6) (2015) 1449–1478.

[24] Q. Yuan, Y. Wu, J. Wang, D. Lu, Z. Zhao, T. Liu, X. Zhang, W. Tan, Targeted bioimaging and photodynamic therapy nanoplatform using an aptamer-guided G-quadruplex DNA carrier and near-infrared light, Angew. Chem. Int. Ed. 52 (52) (2013) 13965–13969.

[25] R. Weissleder, A clearer vision for in vivo imaging, Nat. Biotechnol. 19 (2001) 316.

[26] A.M. Smith, M.C. Mancini, S. Nie, Second window for in vivo imaging, Nat. Nanotechnol. 4 (2009) 710.

[27] S.L. Jacques, Optical properties of biological tissues: a review, Phys. Med. Biol. 58 (11) (2013) R37–R61.

[28] Y. Huang, F. Qiu, L. Shen, D. Chen, Y. Su, C. Yang, B. Li, D. Yan, X. Zhu, Combining two-photon-activated fluorescence resonance energy transfer and near-infrared photothermal effect of unimolecular micelles for enhanced photodynamic therapy, ACS Nano 10 (11) (2016) 10489–10499.

[29] W. Wu, D. Mao, F. Hu, S. Xu, C. Chen, C.-J. Zhang, X. Cheng, Y. Yuan, D. Ding, D. Kong, B. Liu, A highly efficient and photostable photosensitizer with near-infrared aggregation-induced emission for image-guided photodynamic anticancer therapy, Adv. Mater. 29 (33) (2017) 1700548.

[30] Y. Wang, Y. Xie, J. Li, Z.-H. Peng, Y. Sheinin, J. Zhou, D. Oupický, Tumor-penetrating nanoparticles for enhanced anticancer activity of combined photodynamic and hypoxia-activated therapy, ACS Nano 11 (2) (2017) 2227–2238.

[31] M. Wang, Z. Chen, W. Zheng, H. Zhu, S. Lu, E. Ma, D. Tu, S. Zhou, M. Huang, X. Chen, Lanthanide-doped upconversion nanoparticles electrostatically coupled with photosensitizers for near-infrared-triggered photodynamic therapy, Nanoscale 6 (14) (2014) 8274–8282.

[32] G. Chen, H. Qiu, P.N. Prasad, X. Chen, Upconversion nanoparticles: design, nanochemistry, and applications in theranostics, Chem. Rev. 114 (10) (2014) 5161–5214.

[33] H. Qiu, M. Tan, T.Y. Ohulchanskyy, J.F. Lovell, G. Chen, Recent progress in upconversion photodynamic therapy, Nanomaterials 8 (5) (2018) 344.

[34] A. Bagheri, H. Arandiyan, C. Boyer, M. Lim, Lanthanide-Doped upconversion nanoparticles: emerging intelligent light-activated drug delivery systems, Adv. Sci. 3

(7) (2016) 1500437.

[35] Z. Xie, S. Shi, F. Liu, D.L. Smith, P.P. Ruden, C.D. Frisbie, Large magnetoresistance at room temperature in organic molecular tunnel junctions with nonmagnetic electrodes, ACS Nano 10 (9) (2016) 8571–8577.

[36] S.S. Lucky, N. Muhammad Idris, Z. Li, K. Huang, K.C. Soo, Y. Zhang, Titania coated upconversion nanoparticles for near-infrared light triggered photodynamic therapy, ACS Nano 9 (1) (2015) 191–205.

[37] F. Li, Y. Du, J. Liu, H. Sun, J. Wang, R. Li, D. Kim, T. Hyeon, D. Ling, Responsive assembly of upconversion nanoparticles for pH-activated and near-infrared-triggered photodynamic therapy of deep tumors, Adv. Mater. 30 (35) (2018) 1802808.

[38] J. Zuo, L. Tu, Q. Li, Y. Feng, I. Que, Y. Zhang, X. Liu, B. Xue, L.J. Cruz, Y. Chang, H. Zhang, X. Kong, Near infrared light sensitive ultraviolet–blue nanophotoswitch for imaging-guided "off–on" therapy, ACS Nano 12 (4) (2018) 3217–3225.

[39] B. Gu, Q. Zhang, Recent advances on functionalized upconversion nanoparticles for detection of small molecules and ions in biosystems, Adv. Sci. 5 (3) (2018) 1700609-1700609.

[40] L. Xia, X. Kong, X. Liu, L. Tu, Y. Zhang, Y. Chang, K. Liu, D. Shen, H. Zhao, H. Zhang, An upconversion nanoparticle-Zinc phthalocyanine based nanophotosensitizer for photodynamic therapy, Biomaterials 35 (13) (2014) 4146–4156.

[41] C. Tanielian, C. Schweitzer, R. Mechin, C. Wolff, Quantum yield of singlet oxygen production by monomeric and aggregated forms of hematoporphyrin derivative, Free Radical Biol. Med. 30 (2) (2001) 208–212.